Kinetic Monte Carlo approach to Schottky defects in noble metal nanoclusters

Forrest H. Kaatz*† Adhemar Bultheel‡ Ottorino Ori§

Abstract

The vacancy concentration dependence on temperature and diameter of noble metal (gold, silver, and copper) nanoclusters is investigated using a kinetic Monte Carlo method. Icosahedral and decahedral nanoclusters are studied, with diameters up to 3.73 nm for icosahedral clusters and up to 6.65 nm for decahedral clusters. The cohesive energy is calculated using a coordination number approach, resulting in a linear relation with cluster size. Random Schottky defects are frozen into the clusters at low temperatures (100K-600K) and we find that the vacancy concentration increases with smaller diameters and higher temperatures. We develop a model for this behavior, which explains the temperature and size dependence. Vacancy concentrations are related to the ratio of surface/interior sites based on nearest neighbor calculations. The modified enthalpy and entropy of constant diameter clusters are derived from a logarithmic model for the Gibbs energy. Melting entropy and enthalpy are calculated in this coordination type model and compared with previously published molecular dynamics results.

Keywords: vacancy concentration; icosahedra; decahedra; enthalpy; entropy; gold; silver; copper; coordination number; low-atomicity systems

1 Introduction

Defects in solids were first predicted by Frenkel as an interstitial – vacancy pair in 1926 [1]. Wagner and Schottky discussed vacancies, also known as Schottky defects, in a publication in 1930 [2]. Defects can affect the properties of solids, such as luminescence, resistivity, volume and thermal expansion, and affects diffusion and the specific heat [3]. Vacancies are more stable than Frenkel defects since they require less energy of formation in close packed

*Mesalands Community College, 911 South 10th Street, Tucumcari, NM, 88401, USA

†Corresponding author

‡Dept. Computer Sci., KU Leuven, Celestijnenlaan 200A, 3001 Heverlee, Belgium

§Actinium Chemical Research, Via Casilina, 1626/A 00133, Rome, Italy, Laboratory of Computational and Structural Physical-Chemistry for Nanosciences and QSAR,West University of Timişoara, Romania

crystals. Schottky defects are stable in solids since they raise the entropy of the crystal in an Arrhenius model of the Gibbs energy [3]. We will show here that the linear Arrhenius model does not apply to metal nanoclusters, but in fact a logarithmic model takes its place.

Measurements of bulk vacancy concentrations in the noble metals gold, silver and copper were originally done in the early 1960's [4-6]. These were lattice expansion measurements by x-ray diffraction and thermal expansion measurements by micrometer microscopes. A typical concentration in gold at an elevated temperature of 850°C was found to be about $\Delta N/N = 10^{-5}$ [4]. Usually, vacancies are not observed in bulk samples, due to the low concentration and migration of vacancies to grain boundaries and dislocation sinks. However, when heated to near 1000°C and rapidly quenched (4×105°C/sec) to room temperature, vacancy clusters and voids have been seen via electron microscopy in gold after aging at 100°C for one hour [7,8].

Single vacancy and vacancy clusters heavily influence the fundamental properties of materials at the nanoscale and characterizing them, from a theoretical point of view, at the single-defect level represents a scientific investigation of particular relevance. Here, we simulate in nanoclusters of noble metals the effects of individual vacancies placed in lattice sites with different coordination numbers. Our calculations are based on the the Kinetic Monte Carlo (KMC) method is a variant of the Monte Carlo (MC) method specifically designed to model a kinetic approach to fundamental processes and then to study the stochastic sequences giving the temporal evolution of complex systems [9]. It is well suited to study temporal processes that have intermediate time scales, i.e. greater than atomic vibration, along the scale of diffusion, grain growth, and thin-film deposition [9]. It has been used previously in calculations on copper nanoparticles [10]. We use it here to model vacancies in noble metal nanoclusters as a function of size and temperature.

Nanoclusters and nanoparticles are ever increasing scientific fields of study and gold in particular has properties in the nano-regime unknown in the bulk. Silver and copper are more recent scientific studies, as copper is difficult to make due to its rapid oxidation. A nano-phase diagram of structure versus temperature has been developed for gold and silver from experiments and density functional theory (DFT) [11,12]. A phase diagram for copper has been produced as an alloy with gold for nanoclusters [13]. We model all three noble metals, gold, silver, and copper and use gold to present typical data, with tabular data compiled for silver and copper.

The experimental and theoretical work on noble metal nanoclusters goes back to at least 1976 when Buffat and Borel studied gold particles and measured a size dependence in the melting temperatures [14]. For a review of progress in the chemical synthesis and physics of metal nanoclusters, we refer to a publication in 2009 [15]. More recently, work on gold nanoclusters has resulted in atomic structure (icosahedral, decahedral, and fcc) control of isomers during the formation processes [16]. Also tunable size control of gold, silver, and palladium icosahedral clusters has been reported [17]. Silver icosahedral and decahedral clusters have been synthesized in a chemical procedure [18]. Copper icosahedral and decahedral clusters have also been fabricated [19]. Also, of relevance to our analysis, the melting temperatures of gold [14], silver [20,21] and copper [22,23] as a function of cluster size are all above 600K, either experimentally, or by molecular dynamics (MD) calculations.

Property	Gold	Silver	Copper
E_c^b (eV)	3.81 [29]	2.95 [29]	3.49 [29]
Bond length (Å)	2.884 [30]	2.889 [30]	2.556 [30]
G (GPa)	26 [30]	30.3 [30]	48.3 [30]
γ (J/m^2)	1.506 [31]	1.248 [31]	1.8075 [31]
E_v^i (eV)	0.94 [4]	1.09 [5]	1.17 [6]
E_v^σ (eV)	0.494 [32,33]	0.514 [32,33]	0.564 [32,33]
r (nm)	0.134 [30]	0.134 [30]	0.117 [30]

Table 1: Physical properties of the noble metals used in our simulations and references listing these values of the constants.

Metal clusters containing small numbers of atoms N also show catalytic performances of applicative interest. Stable metal particles with enhanced catalytic activity strongly depend on the presence of single atoms or, vice-versa, of single vacancies. Investigations of non-magic-number clusters in noble metals with 'with low atomicity' have just begun, i.e., by exploiting new synthesis methods promising the required single-atom precision in platinum clusters [24]. The results presented here substantially augment the ability to simulate the stability of such low-N metallic nanosystems.

2 Methods

We start with a cluster of N atoms, where the cohesive energy of the particle per atom [25] is

$$E_c^p = E_c^b \left(1 - \frac{C_i - C_\sigma}{C_i} \frac{N_\sigma}{N} \mu\right) \tag{1}$$

here E_c^b is the bulk cohesive energy, C is the coordination number and N the number of atoms. The subscripts i and σ represent interior and surface sites respectively, and μ is the ratio of surface area of the cluster compared to an icosahedron ($\mu = 1$ by definition) [26]. We study icosahedral clusters and decahedral clusters since they have the same surface orientation (111), with 20 and 10 faces for the icosahedra and decahedra, respectively [27]. The surface area of an icosahedron is $5\sqrt{3}$ with unit length between neighbors, while the decahedron has faces as isosceles triangles, with the base in a ratio of about 1.018:1 to the sides [28]. This gives a value of $\mu = 0.506$ for decahedra. The surface and interior atoms in icosahedra and decahedra are separated since the interior atoms have coordination 12 and surface atoms have coordination 9 or less. Thus, as we create vacancies, we count interior atoms as having coordination 10-12 and surface atoms at 9 and below.

For a cluster with N_v vacancies the change in energy is

$$\Delta E_j = E_c^p - \frac{N_v}{N} E_v^p - \frac{N - N_v}{N} E_c^p \quad \text{so for } N_v = 0,\ \Delta E_j = 0 \tag{2}$$

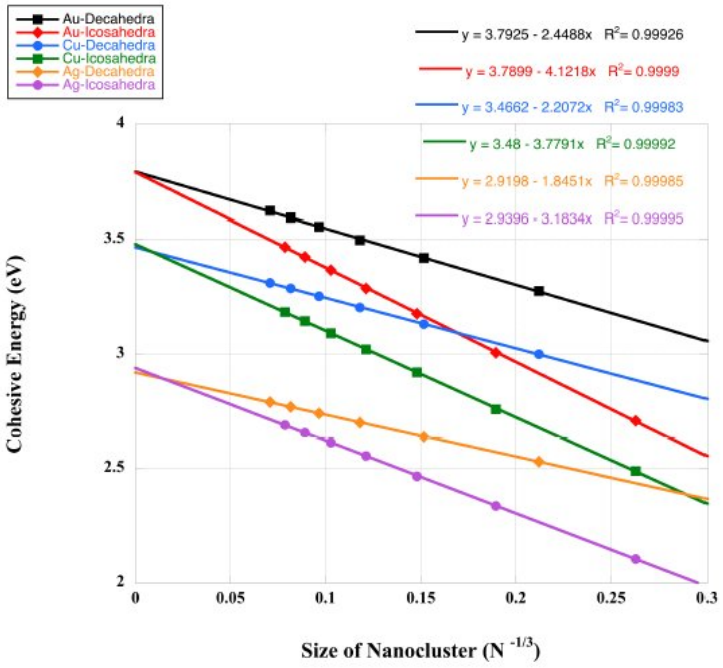

Figure 1: Cohesive energy as a function of cluster size for gold, silver, and copper.

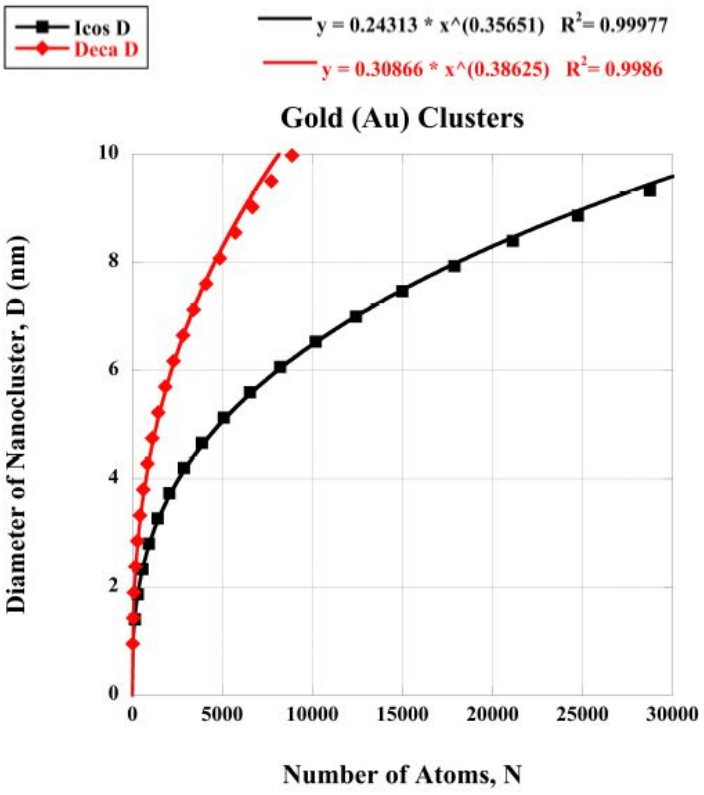

Figure 2: Plot of nanocluster diameter versus number of atoms, N.

However E_v^p depends on a interior or surface site, respectively as

$$E_v^p = \begin{cases} E_v^i\eta + \eta\dfrac{4\pi r^2\gamma^2}{\gamma + 2Gr} - \dfrac{4\pi r^2\gamma_p^2}{\gamma_p + 2Gr} \\ E_v^\sigma\eta + \eta\dfrac{4\pi r^2\gamma^2}{\gamma + 2Gr} - \dfrac{4\pi r^2\gamma_p^2}{\gamma_p + 2Gr} \end{cases} \qquad \begin{cases} \eta = 1 - \dfrac{C_i - C_\sigma}{C_i}\dfrac{N_\sigma}{N}\mu \\ \dfrac{\gamma_p}{\gamma} = 1 - \dfrac{4r}{R}, \end{cases} \tag{3}$$

where γ, R, and r denote bulk surface energy, nanocluster radius, and atomic radius, respectively [25]. Also, E_v^i and E_v^σ are the bulk (interior) and surface (111) vacancy energies of formation. Relevant constants for gold, silver, and copper are listed in Table 1. The concentration of vacancies comes from defining a time interval as:

$$\Delta t = -\frac{\ln\rho}{\sum_i \varepsilon_i}, \quad \text{with } \rho \text{ a random number in } [0,1] \tag{4}$$

where the concentration is defined as:

$$c = \langle c(t)\rangle = \frac{1}{\sum_i \Delta t_i}\sum_i \frac{N_i^v}{N_i^a}\Delta t_i, \quad N_i^a = N - N_i^v. \tag{5}$$

Our modified Metropolis (MC) algorithm for creating a vacancy is then:

0. The structure is initialized with N atoms, without vacancies.

1. Select at random a position p ($1 \le p \le N$).
   If p is an atom then create a vacancy at p. If p is a vacancy then create an atom at p.

   1.1. Compute ΔE_j as in formulas (2) and (3) and $\varepsilon_j = \exp(-\Delta E_j/k_BT)$ for the new configuration (k_B is the Boltzmann constant).

   1.2. Generate a random number $r \in [0,1]$. If a vacancy was created at p and $r > \varepsilon_j$ or an atom was created at p and $r > 1-\varepsilon_j$ then reject this configuration and return to step 1 else accept this configuration and computes Δt and concentration $c(t)$ as in formulas (4) and (5).

   1.3. If the new $c(t)$ value deviates less than 0.5% from the average over the last 100 $c(t)$ values then assume convergence and stop else go to step 1.

2. Repeat 20 times to get an average $c(t)$ for the nanoclusters.

3 Results and discussion

The nanocluster binding energy versus cluster size is plotted for the noble metal clusters in Figure 1. The binding energy is plotted versus magic numbers of the clusters for the two types studied here [34]. This results in a linear relationship with $N^{(-1/3)}$ (the cluster size), similar to what has been calculated from DFT calculations on gold clusters [35]. The slope

for the icosahedra is larger than the decahedra, sinc $\mu = 1$ versus $\mu = 0.506$ for decahedra. This algorithm is efficient and accurately produces the bulk cohesive energy value as the cluster size approaches the bulk limit.

The relationship between D, the cluster diameter and number of atoms is shown in Figure 2. We show calculated diameters, D, from the MATLAB routine, versus magic numbers for icosahedral and decahedral clusters [29]. The curves are for gold clusters at $T = 300K$. These relationships follow a power law with the decahedral clusters having a larger coefficient due to the oblate shape of their geometry in contrast to the near sphericality of icosahedra. The MATLAB routine calculates the largest difference between coordinates in the cluster and an oblate shape will have a greater diameter with a fewer number of atoms.

There are reports in the literature that a central vacancy in icosahedral structures can stabilize metal nanoclusters [35,36]. In Figure 3 we show the energy cost of removing the central atom in noble metal icosahedral clusters in our model according to equation (2). Also shown is the calculation of removing a corner atom from the same clusters. The data follows approximately a curve like $1/N$, with corner atoms having a lower energy cost than the central atom. In this model surface atoms are more easily removed but Figure 4 shows that the energy difference between the central site (Ec) and a corner site (Es) goes to zero at about 1500 atoms. These results indicate that any central vacancy with bulk coordination would behave the same, since this model only takes into account the coordination of the site. This is in contrast to some recent DFT studies, where accounting for strain effects show that a central vacancy may be energetically favored [37]. The data in both figures shows that the energy associated with creating a vacancy depends on the physical parameters of the metals, and for the noble metals goes in order of gold, copper and silver, from largest to smallest.

Figure 5 shows MATLAB plots of icosahedral and decahedral clusters of gold, silver, and copper at $T = 300K$. The vacancies at surface sites are colored green, while vacancies at interior sites are colored blue. These are generated as one possible outcome from a program where some stochastic results are inherent to the method. In Figure 6, we plot the ratio of surface to interior atoms and vacancies in gold clusters which follows a power law behavior as a function of cluster size, D. Other temperatures and metals have similar behavior. This data simply shows the relative number of surface and interior sites as the clusters get larger, and thus changes the number of available sites for random vacancies, with the obvious conclusion that there are more surface sites in smaller clusters.

We change the temperature T and the size of the cluster D, resulting in concentration temperature and diameter profiles as shown in Figure 7. The temperature, T, varies from 100K to 600K, with $D < 3.73$ for icosahedra and $D < 6.65$ for decahedra. We fit the temperature and size profiles to the following function at $T = 600K$:

$$c(T, D) = a_e(T) \exp\left(-\frac{\alpha_e(T) D^{\beta_e}}{k_B T}\right)$$

where e refers to the element modeled (gold, silver, copper). This model is similar to one developed by Guisbiers [38], except that D is in the numerator, rather than the denominator.

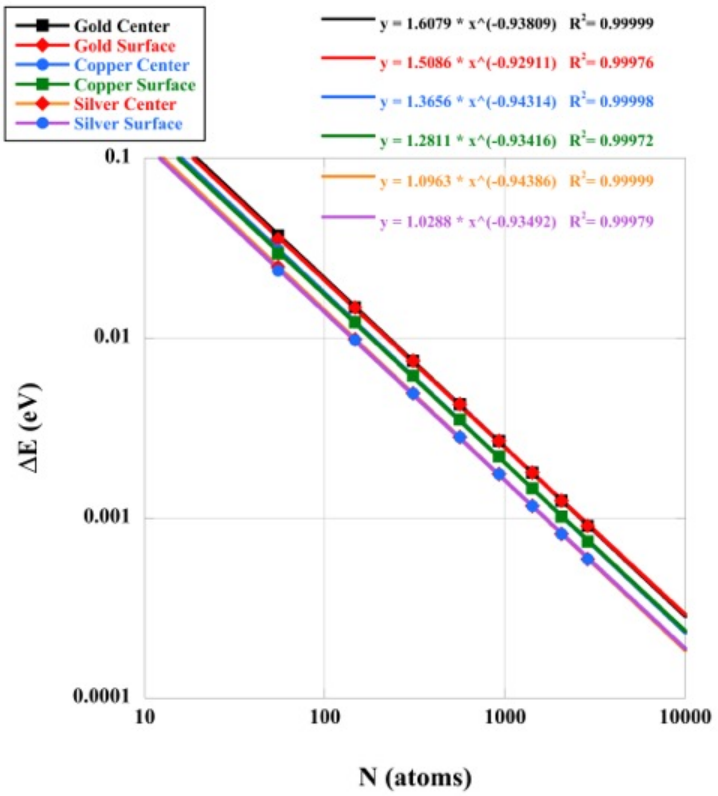

Figure 3: Plots of a single vacancy in icosahedral clusters – in the center and at a corner site.

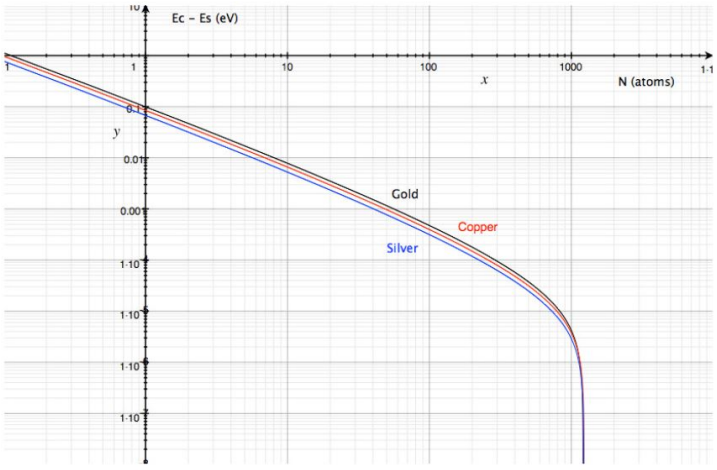

Figure 4: Plots of the energy difference between a central site and a corner site showing that the difference goes to zero at about 2000 atoms.

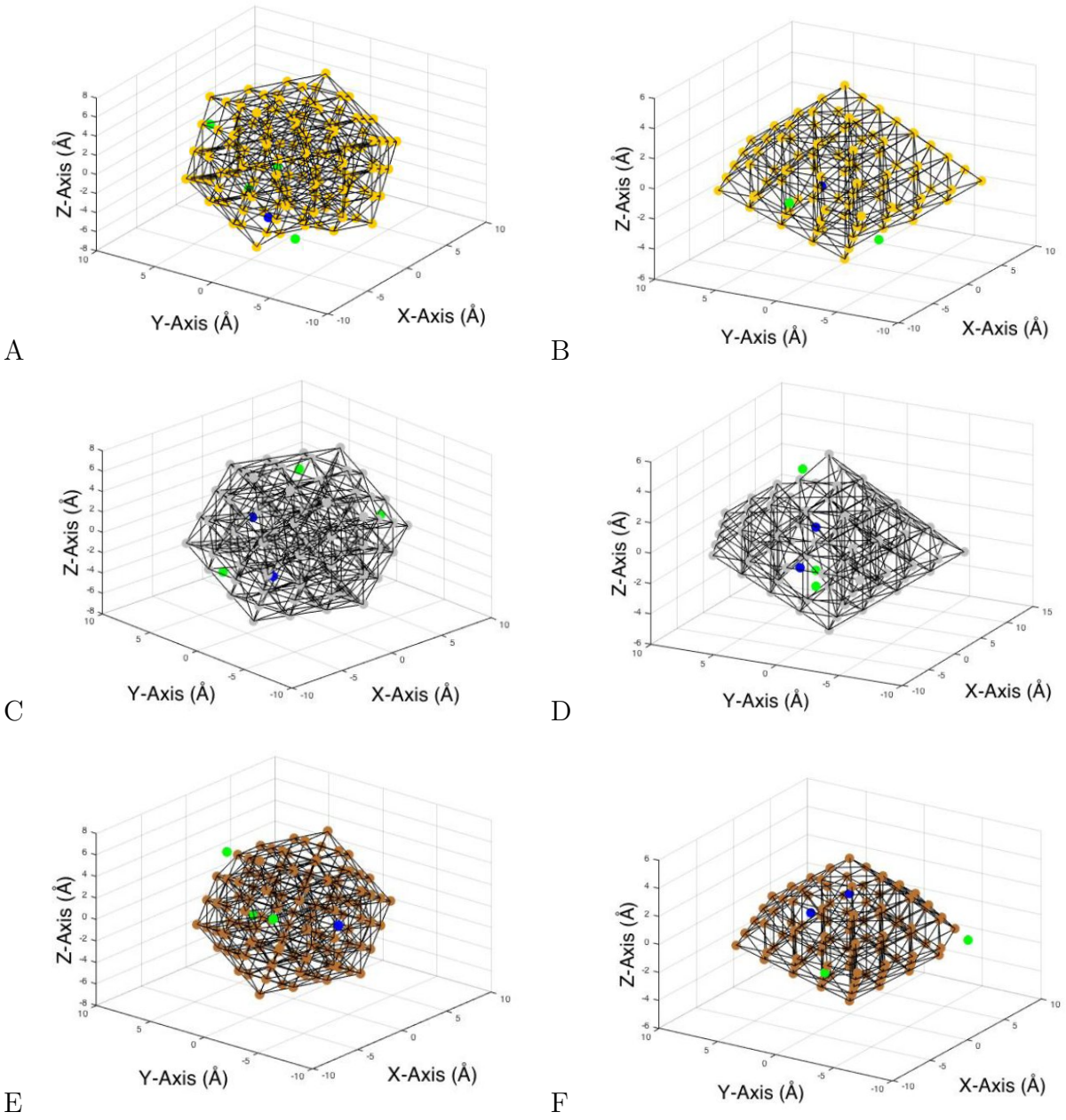

Figure 5: MATLAB plots of gold (A,B), silver (C,D) and copper (E,F) icosahedral and decahedral clusters with surface (green) vacancies and interior (blue) vacancies.

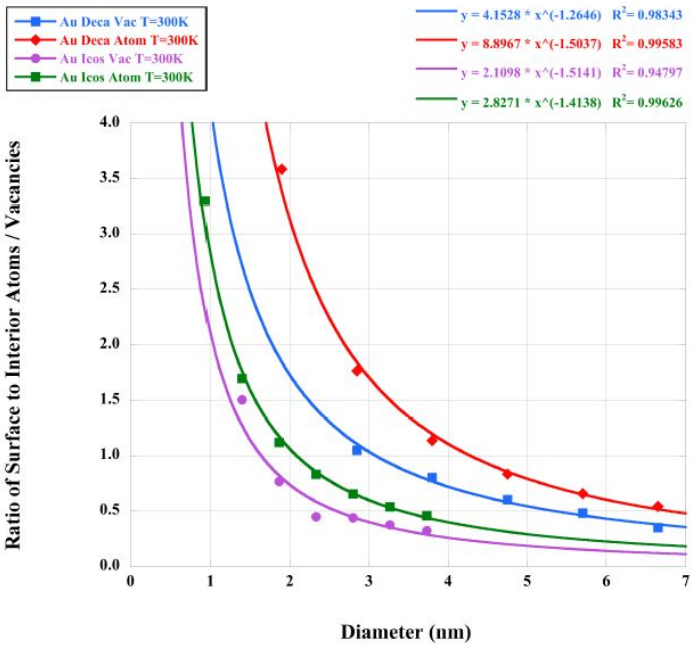

Figure 6: Ratio of surface to interior atoms / vacancies in gold clusters.

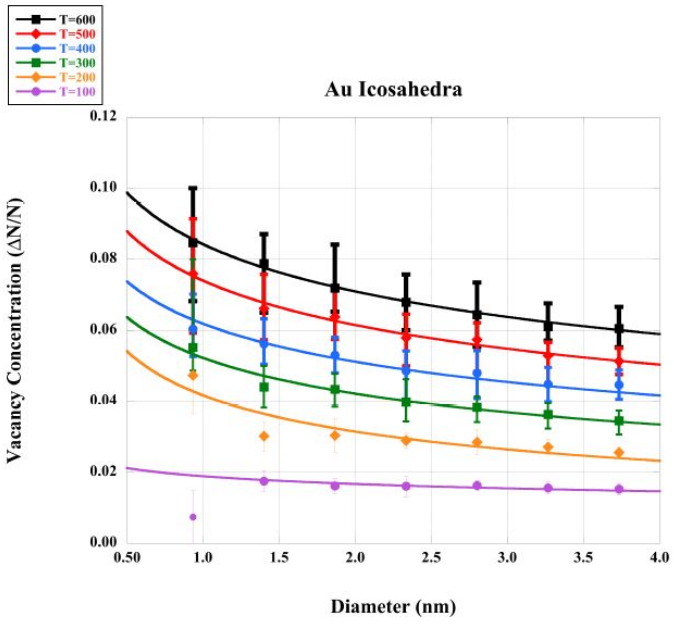

Figure 7: Plots of $c(T, D)$ for gold icosahedra.

For these temperature profiles, we choose $T = 600K$ to fit all three parameters, a_e, α_e, and β_e, then fix β_e for the lower temperatures and determine the best fit for the other ones. In Figure 5, error bars show the minimum and maximum values over the 20 simulations in the algorithm. The average value is taken for the relevant data point in the temperature profile. The data point for $T = 100K$ and $D = 0.9$, is where vacancies are being eliminated from the cluster. The curve fit for the temperature profile $T = 100K$ is without this data point. If we look at the modeling in Table 2 and the variation for the metals, we see that silver clusters have the highest concentration of vacancies, followed by copper, and gold with the lowest. This holds for both icosahedra and decahedra. The evidence indicates that the most important component to $|DeltaE_j$ is E_c^b from equation (1), which results in a higher concentration of vacancies with a low E_c^b. From Table 1, we see that the order of E_c^b is silver, copper, and gold, from low to high, and this produces a reverse order of the vacancy concentration in the metals. Our data which shows that icosahedra have a higher concentration of vacancies than decahedra corroborates this thought since E_c^b is lower for icosahedra than decahedra versus cluster size from Figure 1.

We have found the concentration dependence as a function of D, and the other parameter we vary is the temperature. The temperature analysis starts from a description of the Gibbs energy [39,40] per atom as:

$$G^f = G(c) + k_B T[c \ln c + (1-c)\ln(1-c)]$$

where $G(c)$ is the free energy of a single vacancy and the final term is the configurational free energy of the vacancies. In thermal equilibrium, the concentration $c(T)$ is determined by the condition that the Gibbs energy be a minimum, or $dG^f/dc = 0$. Taking the derivative leads to the following equation:

$$c(T) = \left[\exp\left(\frac{dG(c)}{dc}\frac{1}{k_B T}\right) + 1\right]^{-1}$$

which gives the equilibrium value of the concentration versus Gibbs energy as

$$c(T) = \exp\left(-\frac{G^f}{k_B T}\right), \quad \text{with } G(c) = G_0 + cG^f.$$

In this approximation, we use a linear model for $G(c)$, and $G^f \sim 1\,\text{eV} \gg kBT \sim 1/40\,\text{eV}$ [40]. Now from our data plotted in Figure 8, we have that

$$c(T) = bT + cT^2.$$

or the concentration dependence of metal nanoclusters is quadratic with temperature. We then have our final result that

$$\frac{G_v^f}{k_B T} = -\ln c(T) = -\ln(bT + cT^2) \tag{6}$$

$$\frac{G_v^f}{k_B T} \sim H' - S' \ln T \tag{7}$$

	Icosahedra	Gold	Silver	Copper
$T = 600$	a_e	0.727	0.990	0.780
	α_e	0.111	0.103	0.105
	β_e	0.110	0.159	0.133
$T = 500$	a_e	0.494	1.292	0.922
	α_e	0.0818	0.100	0.099
$T = 400$	a_e	0.436	0.669	0.805
	α_e	0.0673	0.0659	0.0799
$T = 300$	a_e	0.470	0.677	0.536
	α_e	0.056	0.054	0.055
$T = 200$	a_e	0.739	0.572	0.862
	α_e	0.049	0.038	0.049
$T = 100$	a_e	0.038	0.238	0.097
	α_e	0.006	0.016	0.012
	Decahedra	Gold	Silver	Copper
$T = 600$	a_e	0.765	0.987	0.860
	α_e	0.111	0.098	0.104
	β_e	0.098	0.141	0.123
$T = 500$	a_e	0.785	1.333	0.871
	α_e	0.099	0.099	0.091
$T = 400$	a_e	0.470	0.906	0.651
	α_e	0.069	0.073	0.0702
$T = 300$	a_e	0.407	1.032	0.694
	α_e	0.053	0.062	0.0589
$T = 200$	a_e	0.106	0.462	0.254
	α_e	0.020	0.034	0.028
$T = 100$	a_e	0.432	0.411	0.798
	α_e	0.024	0.020	0.026

Table 2: Fitting parameters to the $c(T, D)$ model discussed in the text.

	Icosahedra	Gold	Silver	Copper
$D = 1\,\mathrm{nm}$	H'	7.748	6.800	7.322
	S'	0.832	0.753	0.796
$D = 2\,\mathrm{nm}$	H'	7.763	6.997	7.386
	S'	0.802	0.745	0.770
$D = 3\,\mathrm{nm}$	H'	7.788	7.123	7.426
	S'	0.795	0.740	0.754
	Icosahedra	Gold	Silver	Copper
$D = 1\,\mathrm{nm}$	H'	7.395	6.920	6.829
	S'	0.750	0.750	0.698
$D = 2\,\mathrm{nm}$	H'	7.615	7.232	7.282
	S'	0.761	0.762	0.740
$D = 3\,\mathrm{nm}$	H'	7.751	7.429	7.566
	S'	0.768	0.769	0.767

Table 3: Modified enthalpy and entropy for icosahedral and decahedral clusters for gold, silver, and copper.

where H' and S' are independent of T and we have plotted the logarithm of the concentration versus temperature in Figure 9 for gold nanoclusters. The constant diameter values for the data points comes from the curve fitting we have done in Figure 7. Plots of equations (6) and (7) will produce nearly overlapping functional dependencies, if the generated curve fits are used, and we use the simpler equation (7) for modeling purposes. We emphasize here that this is strictly a fitted model without a physical derivation. Additionally, this fit only holds for $T \geq 0$K, which should not be a problem, as absolute zero is not actually physically reached. In Table 3, we list the values of the modified enthalpy, H', and entropy S', which are dimensionless, for the two types of clusters and the three noble metals we have studied. Since gold has the lowest concentration from Table 2, it has the highest value for H' and S'. The linear Arrhenius model assumes a functional form for the Gibbs energy as $G^f(T) = H^f - S^f T$, with H^f and S^f the temperature independent experimentally determined enthalpy and entropy, respectively, but this does not fit our data or model. We mention here that non-linearity of the Gibbs energy has been seen in bulk behavior, where a quadratic model was used [41]. Our model has determined the complete temperature dependence from 100K to 600K, and thus there are no gaps in the data, as is seen from DFT calculations of bulk behavior [41].

The melting entropy and enthalpy can be calculated in this coordination type model as follows:

$$S_m^p - S_m^b + \frac{3R}{2}\ln\eta, \quad H_m^p = \eta\left(H_m^b + \frac{3R}{2}T_m^b \ln\eta\right)$$

where T_m^b, S_m^b and H_m^b are the bulk melting temperature, entropy and enthalpy, R is the universal gas constant, and η is defined as in equation (3) [40]. The constants for silver and

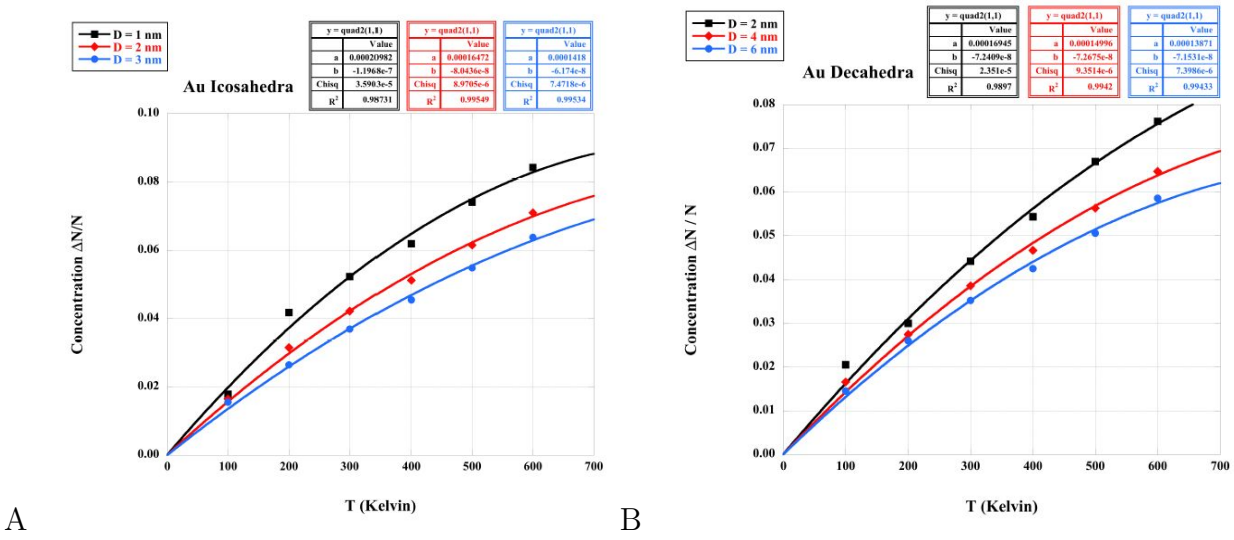

A B

Figure 8: Quadratic plots of concentration versus temperature for gold clusters. A. Icosahedra B. Decahedra.

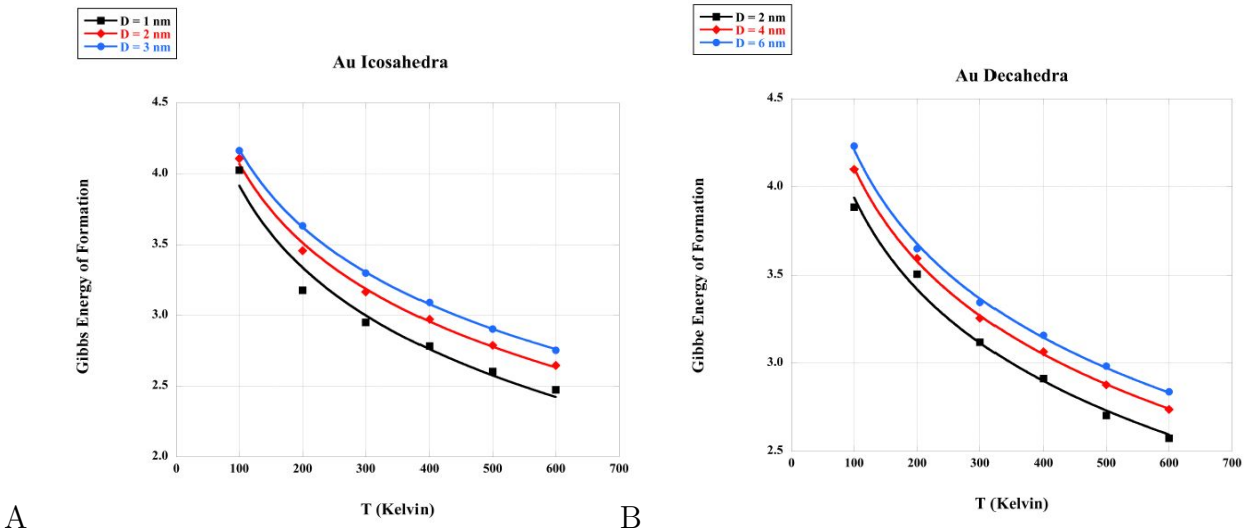

A B

Figure 9: Plots of the logarithm of concentration as a function of temperature for gold clusters. A. Icosahedra B. Decahedra.

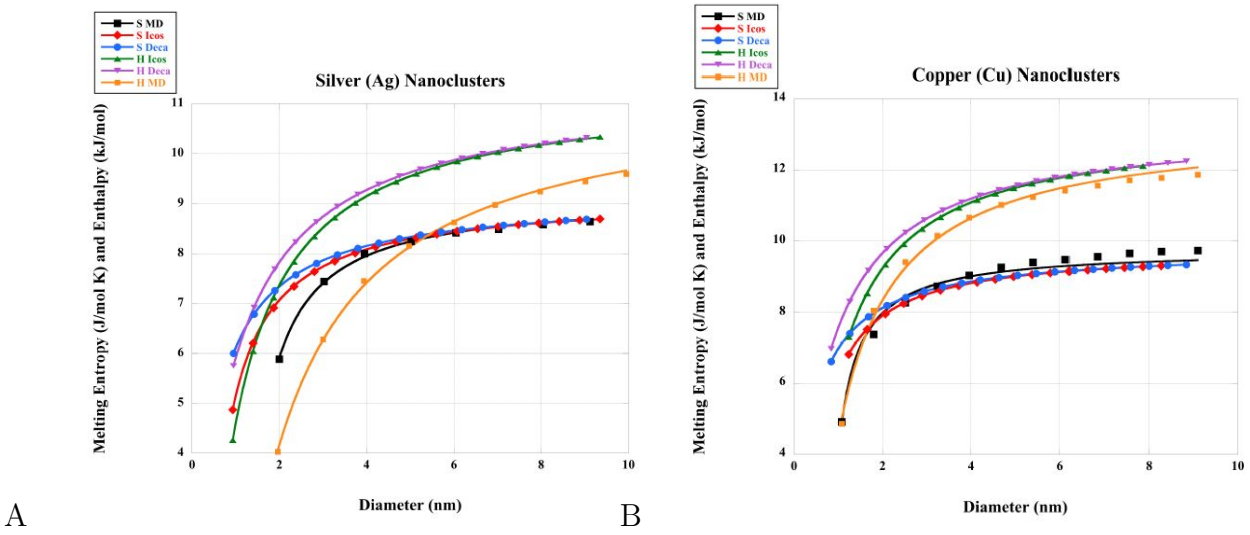

Figure 10: Calculated melting entropy and enthalpy data for A. Silver and B. Copper clusters, plotted with MD results. MD results for silver are from [41] and copper from [22].

copper are given in Table 4. In Figure 8, we plot the melting entropy and enthalpy versus cluster diameter for silver icosahedral, decahedral, and MD calculations [41]. The curves are fit using equations as

$$S_m^p = S_m^b + \frac{3R}{2} \ln\left(1 - \left(\frac{a}{b+D}\right)\right)$$

$$H_m^p = H_m^b \left(1 - \left(\frac{a}{b+D}\right)\right)\left(1 + \frac{3R}{2S_m^b} \ln\left(1 - \left(\frac{a}{b+D}\right)\right)\right)$$

where a and b are fitting parameters and the relationship in parentheses represents η [44]. We see from Figure 8A that the melting entropy is closely modeled for $D < 4\,\text{nm}$, while the calculated melting enthalpy overestimates the MD results. The results for copper are plotted in Figure 10B. The calculated entropy underestimates the MD results [22], while the calculated enthalpy overestimates the MD results. For both the silver and copper cases, the calculated results are better for icosahedra than decahedra. Table 5 lists the fitting parameters for the MD and calculated entropy and enthalpy data. We are not aware of entropy and enthalpy MD data for gold as a function of diameter.

In this model, random vacancies are frozen into the nanoclusters, making detection of these defects difficult. Recently, three-dimensional imaging of gold clusters [45-48] has been realized and these may well be model systems for detection of defects in the clusters. One of these references showed the existence of adatoms on gold nanocluster surfaces [44]. If adatoms are created through the formation of a vacancy – adatom pairs, then such clusters may have vacancies below the surface. Another possibility is to study the nano behavior of the clusters between an STM tip, the cluster, and a substrate, in an attempt to study

Element	Melting T_m^b	Melting S_m^b	Melting H_m^b
Silver	1234.93 K	9.148 J/(mol K)	11.297 (kJ/mol)
Copper	1357.77	9.768 J/(mol K)	13.263 (kJ/mol)

Table 4: Bulk melting thermodynamic data for silver and copper

Thermo Data	Ag a	Ag b	Cu a	Cu b
Entropy MD	0.3033	−0.6790	0.2109	−0.4320
Entropy Icos	0.3489	0.2652	0.3119	0.2372
Entropy Deca	0.3572	0.6473	0.3215	0.5944
Enthalpy MD	0.6294	0.1265	0.3676	0.1318
Enthalpy Icos	0.3528	0.2768	0.3118	0.2365
Enthalpy Deca	0.3623	0.6677	0.3214	0.5932

Table 5: Fitting parameters for MD and calculated entropy and enthalpy data.

defects. Such approaches could well lead to new insights into the defects in these systems.

Conclusion

In summary, we have determined the size and temperature dependence of the concentration of Schottky defects in noble metal nanoclusters. We have modeled this behavior using a kinetic Monte Carlo approach, producing new equations in both the size and temperature profiles. According to this model, silver icosahedra should have the highest concentration of vacancies in the noble metal clusters studied. The Gibbs energy is shown to have a logarithmic dependence, and we have extracted modified enthalpy and entropy coefficients for the clusters. Reasonable agreement of the calculated melting entropy and enthalpy is found with molecular dynamics data. Gold nanoclusters may well be ideal systems for observing these defects, with progress being made to study these clusters.

Acknowledgments

The MATLAB file Cluster Generator available from MATLAB Central was invaluable in assisting the simulation of Schottky defects in these clusters. We thank the reviewers and editor for suggestions that improved the manuscript.

References

[1] J. Frenkel, Thermal movement in solid and liquid bodies, *Z. Phys.* **35** (8/9), (1926) 652-669.

[2] C. Wagner and W. Schottky, Theory of controlled mixed phases, *Z. Phys. Chem.* **11** (2/3), (1930) 163-210.

[3] Y. Kraftmakher, Equilibrium vacancies and thermophysical properties of metals, *Phys. Rep.* **299**, (1998) 79-188.

[4] Simmons, R.O.; Balluffi, R.W. Measurement of equilibrium concentrations of lattice vacancies in gold, *Physical Review* **125**(3), (1962), 862-872.

[5] Simmons, R.O.; Balluffi, R.W. Measurement of equilibrium concentrations of lattice vacancies in silver near the melting point, *Physical Review* **119**(2), (1960), 600-605.

[6] Simmons, R.O.; Balluffi, R.W. Measurement of equilibrium concentrations of vacancies in copper, *Physical Review* **129**(4), (1963), 1533-1544.

[7] Mori, T.; Meshii, M. On the nucleation of vacancy clusters in gold, *Acta Metallurgica* **12**, (1964) 104-106.

[8] Uefuji, T.; Shimomura, Y.; Kimo, T. Formation of vacancy clusters in quenched pure gold and gold dilute alloys, *Japanese Journal of Applied Physics* **16**(6), (1977) 909-918.

[9] C.C. Battaile, The Kinetic Monte Carlo method: foundation, implementation and application, *Computational Methods in Applied Mechanical Engineering* **197**, (2008) 3386-3398.

[10] M. Müller, and K. Albe, Concentration of thermal vacancies in metallic nanoparticles, *Acta Materialia* **55** (2007) 3237-3244.

[11] A.S. Barnard, N.P Young, A.I. Kirkland, M.A. van Huis, and H. Xu, Nanogold: a quantitative phase map, *ACS Nano* **3**(6), (2009) 1431-1436.

[12] A.L. Gonzalez, C. Noguez, J. Beranek, and A.S. Barnard, Size, shape, stability and color of plasmonic silver nanoparticles, *Journal of Physical Chemistry C* **118** (2014), 9128-9136.

[13] G. Guisbiers, S. Mejia-Rosales, S. Khanal, F. Ruiz-Zepeda, R.L. Whetton, and M.J. Yacaman, Gold-copper nano-alloy, 'Tumbaga', in the era of nano: phase diagram and segregation, *Nano Letters* **14**, (2014) 6718-6726.

[14] Ph. Buffat and J-P. Borel, Size effect on the melting temperature of gold particles, *Physical Review A* **13**(6), (1976) 2287-2298.

[15] Y. Xia, Y. Xiong, B. Lim, and S.E. Skrabalak, Shape-Controlled Synthesis of Metal Nanocrystals: Simple Chemistry Meets Complex Physics?, *Angew. Chem. Int. Ed.* **48**, (2009) 60-103.

[16] S.R. Plant, L. Cao, and R.E. Palmer, Atomic Structure Control of Size-Selected Gold Nanoclusters during Formation, *J. Am. Chem. Soc.* **136**, (2014) 7559-7562.

[17] Q. Zhang, J. Xie, J. Yang, and J.Y. Lee, Monodisperse Icosahedral Ag, Au and Pd Nanoparticles: Size Control Strategy and Superlattice Formation, *ACS Nano* **3**(1), (2009) 139-148.

[18] M. Tsuji, M. Ogino, R. Matsuo, H. Kumagae, S. Hikino, T. Kim, and S.H. Yoon, Stepwise Growth of Decahedral and Icosahedral Silver Nanocrystals in DMF, *Crystal Growth and Design* **10**, (2010) 296-301.

[19] F. Silly and M.R. Castell, Temperature-Dependent Stability of Supported Five-Fold

Twinned Copper Nanocrystals, *ACS Nano* **3**(4), (2009) 901-906.

[20] I. Shyjumon, M. Gopinadhan, O. Ivanova, M. Quaas, H. Wulff, C.A. Helm, and R. Hippler, Structural Deformation, melting point and lattice parameter studies of size selected silver clusters, *Eur. Phys. J. D* **37**, (2006) 409-415.

[21] H.A. Alarifi, M. Atis, C. Ozdogan, A. Hu, M. Yavuz, and Y. Zhou, Determination of Complete Melting and Surface Premelting Points of Silver Nanoparticles by Molecular Dynamics Simulation, *J. Phys. Chem. C*, **117**(23) 12289-12298.

[22] F. Delogu, Structural and energetic properties of unsupported Cu nanoparticles from room temperature to the melting point: Molecular dynamics simulations, *Physical Review B* **72**, (2005) 205418.

[23] H.H. Kart, H. Yildirim, S. Ozdemir Kart, and T. Cagin, Physical Properties of Cu Nanoparticles: A Molecular Dynamics Study, *Materials Chemistry and Physics* **147**, (2014) 204-212.

[24] Imaoka, T., Kitazawa, H., Chun, W.-J. and Yamamoto, K. Finding the most catalytically active Platinum clusters with low atomicity. *Angew. Chem. Int. Ed.* **54**, (2015) 9810–9815.

[25] H. Delavari H., H. Madaah Hosseini, and A. Simchi, A simple model for the size and shape dependent Curie temperature of freestanding Ni and Fe nanoparticles based on the average coordination number and atomic cohesive energy, *Chemical Physics* **383**, (2011) 1-5.

[26] H. Delavari H., H.R.M. Hosseini, and A. Simchi, Effects of particle size, shape, and crystal structure in freestanding metal nanoparticles: a model study, *Physica B* **406**, (2011), 3777-3780.

[27] G. Guisbiers and G. Abudukelimu, Influence of nanomorphology on the melting and catalytic properties of convex polyhedral nanoparticles, *Journal of Nanoparticle Research* **15**, (2013) 1431.

[28] A. Cervellino, C. Giannini, and A. Guagliardi, Determination of nanoparticle structure type, size, and strain distribution from X-ray data for monatomic f.c.c-derived non-crystallographic nanoclusters, *Journal of Applied Crystallography* **36**, (2003) 1148-1158.

[29] C. Kittel, *Introduction to Solid State Physics*, Eighth Edition, John Wiley and Sons, Inc, Hoboken, NJ, 2005.

[30] W. Martienssen and H. Warlimont, *Springer Handbook of Condensed Matter and Materials Data*, Springer: Berlin, 2005.

[31] Jiang, Q.; Lu, H.M. Size dependent interface energy and its applications, *Surface Science Reports* **63**, (2008) 427-464.

[32] Zhang, J.M.; Song, X.L.; Zhang, X.J.; Xu, K.W.; Ji, V. Atomistic simulation of point defects at low-index surfaces of noble metals, *Surface Science* **600** (2006) 1277-1282.

[33] Andreev, Y.Y. Thermodynamic calculations of surface energy and energy of adatom and surface vacancy formation for face-centered cubic metals, *Russian Journal of Physical Chemistry* **79**(2), (2005), 179-185.Z defects at low-index surfaces of noble metals, *Surface Science* **600** (2006) 1277-1282.

[34] F.H. Kaatz and A. Bultheel, Topological indices for nanoclusters, *Computational Materials Science* **99**, (2015) 73-80.

[35] C. Mottet, G. Treglia, and B. Legrand, New magic numbers in metallic clusters: an unexpected metal dependence, *Surface Science* **383**, (1997) L719-L727.

[36] X. Shao, Y. Xiang, and W. Cai, Formation of the central vacancy in icosahedral Lennard-Jones clusters, *Chem. Phys.* **305**, (2004) 69-75.

[37] H. Li, L. Li, A. Pederson, Y. Gao, N. Khetrapal, H. Jonsson and X.C. Zeng, Magic-Number Gold Nanoclusters with Diameters from 1 to 3.5 nm: Relative Stability and Catalytic Activity for CO Oxidation, *Nano Letters* **15**, (2015) 682-688.

[38] G. Guisbiers, Schottky defects in nanoparticles, *Journal of Physical Chemistry C* **115**, (2011) 2616-2621.

[39] G.A. de Wijs, G. Kresse, and M.J. Gillan, First order phase transitions by firstprinciples free energy calculations: The melting of Al, *Physical Review B* **57**(14), (1998) 8223-8234.

[40] D. Fuks and S. Dorfman, Thermodynamics of the atom-vacancy solid solution from a self-diffusion Arrhenius plot, *Physical Review B* **50**(22), (1994) 16340-16345.

[41] A. Glensk, B. Grabowski, T. Hickel, and J. Nuegebauer, Breakdown of the Arrhenius law in describing vacancy formation energies: the importance of local anharmonicity revealed by Ab initio thermodynamics, *Physical Review X* **4**, (2014) 011018.

[42] H. Omid, H. Delavari H.,and H. R. M. Hosseini, Melting Enthalpy and Entropy of Freestanding Metallic Nanoparticles Based on Cohesive Energy and Average Coordination Number, *J. Phys. Chem. C* **115**, (2011), 17310–17313.

[43] W. Luo, W. Hu, and S. Xiao, Size Effect on the Thermodynamic Properties of Silver Nanoparticles, *J. Phys. Chem. C* **112** (2008), 2359-2369.

[44] M.A. Sandiz and A. Safaei, Melting Entropy and Enthalpy of Metallic Nanoparticles, *Materials Letters* **62**, (2008), 3954-3956.

[45] Z.W. Wang, and R.E. Palmer, Mass spectrometry and dynamics of gold adatoms observed on the surface of size-selected Au nanoclusters, *Nano Letters* **12**, (2012) 91-95.

[46] M. Azubel, J. Koivisto, S. Malola, D. Bushnell, G.L. Hura, A.L. Koh, H. Tsunoyama, T. Tsukuda, M. Pettersson, H. Hakkinen and R.D. Kornberg, Electron microscopy of gold nanoparticles at atomic resolution, *Science* **345** (2014) 909-912.

[47] D. Bahena, N. Bhattarai, U. Santiago, A. Tlahuice, A. Ponce, S.B.H. Bach, B. Yoon, R.L. Whetton, U. Landman, and M.J. Yacaman, STEM electron diffraction and highresolution images used in the determination of the crystal structure of the Au144(SR)60 cluster, *Journal of Physical Chemistry Letters* **4**, (2013) 975-981.

[48] Z.Y. Li, N.P. Young, M. Di Vece, S. Palomba, R.E. Palmer, A.L. Bleloch, B.C. Curley, R.L. Johnston, J. Jiang and J. Yuan, Three-dimensional atomic-scale structure of size-selected gold nanoclusters, *Nature* **451**, (2008), 46-49.